

A Detailed Fluid Mechanical Analysis on Pressure Relief Valve Blowdown

Péter Sáfrány¹, Csaba Hős^{1*}

¹ Department of Hydrodynamic Systems, Faculty of Mechanical Engineering, Budapest University of Technology and Economics, Műegyetem rkp. 3., H-1111 Budapest, Hungary

* Corresponding author, e-mail: hos.csaba@gpk.bme.hu

Received: 06 December 2024, Accepted: 30 January 2025, Published online: 10 February 2025

Abstract

We study the root cause behind pressure relief valve blowdown, i.e. the difference in opening and reseating pressure. Simple disc valve geometries with an adjustment ring are studied, with and without a deflecting skirt on the valve body, for incompressible fluid. An analytical estimate is given for the fluid force acting on the valve body, which considers both the uneven pressure distribution and the momentum force due to fluid deflection, the former being the principal driving mechanism of blowdown. Computational Fluid Dynamics computations reveal that the flow is close to ideal and prove the validity of the assumptions behind the analytic results. It was found that the skirt deflecting the outlet flow is indispensable to generating blowdown; however, its role is not in the additional momentum force due to varying the exit jet angle of the flow, but in increasing the pressure at the outer radii due to its orifice effect.

Keywords

pressure relief valve, blowdown, adjustment ring, CFD

1 Introduction

1.1 Background and motivation

Pressure relief valves (PRVs) are essential safety devices employed across various industrial applications to mitigate the risks associated with overpressure conditions in systems such as boilers, pipelines, and storage tanks. These valves automatically discharge excess pressure, protecting equipment integrity and personnel safety from potential hazards, including explosions and leaks. Malfunctioning of such valves leads to catastrophic events; see [1] for a well-documented recent example.

When designing or selecting a pressure relief valve, the key parameters to be considered to ensure safe and effective performance are

- set pressure, i.e. the point at which the relief valve opens to relieve excess pressure,
- relief capacity, i.e. the maximum flow rate the valve can discharge to prevent system overpressure and
- blowdown or reseating pressure, i.e. the percentage drop in pressure needed after valve opening for it to reseat.

An appropriate blowdown setting prevents the valve from chattering (rapid opening and closing), ensures

stability during relief events and allows complete pressure relief. Adjustable blowdown settings (via the so-called adjustment ring) are often provided for critical applications where precise control is necessary.

It is remarkable that PRVs allow different opening (set) pressure and re-closing (reseat, blowdown) pressures without any external control or energy source, purely based on classical mechanics, which makes them ideal for safety-critical applications. However, the exact mechanism of blowdown is less understood, as we shall show in the next section.

1.2 Literature review

Modelling attempts on the dynamical behaviour of PRV date back to the 1980s; one of the first such models was suggested in [2], where both the pressure and momentum force were taken into account (see Section 2.1 more details). Ray in [3] modelled the pressure and momentum forces combined by defining an "effective area". On the contrary, Singh achieved the "popping" action of the valve (that is, sudden opening once the upstream pressure reaches the set pressure) by increasing the inlet area (A_1) by 20% (denoted by A_2) once the valve started to open. The very same increased pressure area resulted in a lower reseat pressure (blowdown) in

a natural manner. This paper not only demonstrated that increased backpressure results in valve instability (chatter) but also showed that varying the adjustment ring (see Fig. 1) changes the angle of the outlet jet (θ) and hence the net overall force. The same modelling mechanism (increased pressure area if the valve is open and varying jet angle to cope with the change of the momentum force) was used in later studies, notably in Darby's papers [4–6].

In [7] the authors share experimental results on the flow and force coefficients of poppet and disc valve geometries. Based on flow visualization results, they conclude that "In some cases, the Coanda effect would cause the jet to curve and attach itself either to the poppet seat or to the poppet stem guide" and also cite further experimental results on different flow patterns. The fact that the flow might not follow the geometry as "expected" makes using the θ jet angle cumbersome. More importantly, they show experimentally that in the case of a disc valve, the overall fluid force for small valve openings is *smaller* than the opening force (see Fig. 8 in [7]). In other words, the "effective" pressure area decreases for small openings and only starts to increase when the valve reaches moderate openings. In [3], the author already use the term *effective area* and defines it as a function of the (normalized) valve lift. However, it is also stated that "A is a strictly monotonically increasing function of, i.e. the effective area of the valve disc increases as the valve rises", which contradicts the experimental findings in [7].

With the advent of computational fluid dynamics (CFD) techniques, valve modelling studies gained new momentum as software allowed for detailed flow field investigations under steady and unsteady conditions. One of the first CFD studies focusing on blowdown prediction is [8], in which the effective area curve (denoted by C_p) is computed utilizing steady-state computations, which is then fed into a simplified dynamical model, i.e. the equation of motion of the

valve. The effective area is assumed to be independent of the pressure level and described by a simple $C_f(x)$ relationship (using the original notation). In [9], fully dynamical CFD computation is performed via the moving mesh technique and a detailed description is given on the flow field. More importantly, instability is found upon closing, its presence being independent of the vessel size (see Fig. 17 in [9]). The effect of the adjusting ring position on the blowdown is also studied, and the CFD results are in good agreement with the experiments. Another study from the same authors [10] proves that the opening process (popping) can also be captured by CFD, despite the small gaps and the potential change in the mesh topology when the valve closes. It is also relatively straightforward to incorporate more complex physical and geometrical scenarios in CFD, e.g. [11] studies the case of two adjustment rings and steam as a working medium. The importance of careful CFD settings (turbulence model, near-wall treatment, grid resolution, etc.) must also be stressed, as in [12, 13]. Efforts have also been made to replace the high-fidelity but case-specific and time-consuming CFD computations employing a lower number of CFD runs and then use response surface methods to predict the effect of parameters, see [14]. Finally, in [15] the authors perform a purely CFD analysis on the effect of the adjusting ring position, similar to the present study.

Acoustic interaction between the valve and the upstream or downstream piping as a potential source of instability and valve chatter was also reported in the literature. In [16], the authors report severe piston oscillations in a field application with natural gas, which was replicated in a lower-pressure test rig and with a predictive mathematical model with a standard PRV model connected to a one-dimensional solver to capture the pipeline dynamics (which provides a computationally efficient alternative for pipe modelling). This work also modelled the fluid forces with the effective area approach (see Fig. 9 in [16]). Another study [13] reveal that the fluid force vs. lift curve can be highly non-trivial even for simple geometries. Experimental studies with two-phase flows also reveal that the effective area curve is relatively insensitive to the liquid mass fraction in airflow (see [17, 18]). Even though it is relatively trivial, it is interesting that the relationship between the effective area curve (fluid force) and the spring rate (or spring force) earned little attention; one of the few papers emphasising its importance is [18]. As we shall see later in this paper, comparing these forces provides a clear and versatile tool to explain several aspects of the behaviour of PRVs.

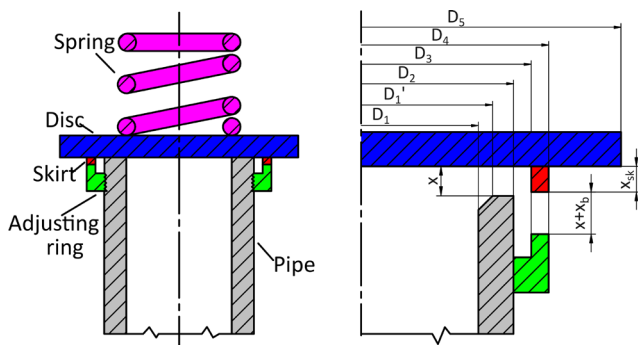


Fig. 1 Valve geometry with adjustment ring and skirt. x stands for valve opening, x_{sk} is the skirt height and x_b is the adjustment ring setting, with $x_b = 0$ being the adjustment ring's uppermost position.

1.3 Aims and structure of the study

This study aims to explain the blowdown effect by analysing the fluid force vs. lift curve of the valve and, based on that, deriving the lift vs. pressure behaviour. In particular, we study two idealized but typical geometries: disc valve bodies with and without a skirt in the presence of an adjustment ring (see Fig. 1). In Section 2, we provide a general theoretical description of the valve-lift curve and explain via synthetic effective area curves the popping and blowdown nature of the valves (unlike purely CFD-based studies such as e.g. [15]). In Section 3, the Computational Fluid Dynamics technique is used to analyse the flow field and pressure distribution for different adjustment ring settings, with and without a skirt. As will be shown, the skirt's presence fundamentally impacts the valve's behaviour. Finally, we conclude the study in Section 5.

2 Theory

2.1 Valve model

The valve body, the spindle and the spring form a 1-degree-of-freedom oscillatory system with the following equation of motion:

$$m\ddot{x} + k\dot{x} + s(x + x_0) = F_f := A_{eff}(x) A_x \Delta p \quad (1)$$

where m is the mass of the interacting bodies, x , \dot{x} and \ddot{x} are the displacement, velocity and acceleration of the valve, k is the viscous damping factor, x_0 is the spring stiffness. F_f is the fluid force acting on the valve body, which will be described by the effective area A_{eff} (yet to be defined in detail) based on the reference surface A_x . Δp denotes the pressure drop through the valve, practically measured at the flanges. For most of this paper, the viscous damping k represents the unmodelled but unavoidable natural damping effects and is estimated to be 1% of the critical damping. Gravity was also neglected in the above equation of motion.

The effective surface area $A_{eff}(x)$ is the axial flow force measured on the valve stem for a given static valve opening $x(x = 0)$ and pressure drop, divided by the static pressure difference measured on the valve. It is a similar concept to the one introduced in [7], where $f_F = 1 - F / (A_1 \Delta p)$. Thus, we do not separate the force components from the pressure distribution, the momentum variation of the flowing medium and the sliding stress distribution, such as [4, 8, 16, 19–22] or [23]. Although this description may seem to be an oversimplification, it is practical and greatly simplifies the modelling of flow forces; for example, it does not require a detailed study of the internal arrangement and geometry of the valve and the difficult-to-measure pressure p_s (see Fig. 1). The drawback is

that determining the $A_{eff}(x)$ curve requires measurements and/or numerical simulation. At the same time, the experiments require easy, directly measurable quantities (force and displacement), unlike, e.g. Darby's [4] model, where the exit angle of the fluid as a function of valve opening is *incoming* data in the model. The issue of the effective surface area is discussed in detail in this section, emphasizing that this curve can, in most cases, be described with sufficient accuracy as a function of valve openness alone and that the effect of pressure difference is secondary only.

The valve must open at a preset opening pressure p_{set} , hence

$$s x_0 = A_{eff}(0) A_1 p_{set}. \quad (2)$$

p_{set} is *gauge* pressure (relative to ambient pressure), whereas all other pressure values are absolute pressures throughout this work.

With increasing inlet pressures, the opening also increases, and such valves are typically designed to reach their maximum opening at 110% of the set pressure, thus

$$s(x_0 + x_{max}) = A_{eff}(x_{max}) 1.1 \times p_{set}. \quad (3)$$

For an incompressible fluid, the flow rate is

$$\dot{m} = C_d(x) A_{ft}(x) \sqrt{2\rho\Delta p}, \quad (4)$$

where $C_d(x)$ is the discharge coefficient (see e.g. [24, 25]) and $A_{ft}(x)$ is the flow-through area:

$$A_{ft}(x) := D_2 \pi x, \quad (5)$$

see Fig. 1. Let us define the dimensionless (relative) opening $\tilde{x} = x / (D_2/4)$. Note that if $D_1 \approx D_2$, $\tilde{x} \approx 1$ is the opening for which the flow-through equals the inlet piping cross-section. In other words, for $\tilde{x} > 1$, the choke area is the inlet piping and not the curtain area behind the valve body.

2.2 Valve characteristic curve

In what follows, we shall derive the characteristic curve of the valve, i.e. the pressure-lift relation. The force model defined by Eq. (1) is *static*, i.e. it does not consider the dynamic forces generated during the movement of the valve similar to the corresponding literature (see e.g. [6, 26–28]).

As a simple example, let us consider the case of a simple disc valve with piping diameter D_1 of negligible thickness. We have

$$F_f = A_1 \Delta p + \dot{m} v_1 = A_1 \Delta p \left(1 + 2C_d(x)^2 \left(\frac{4x}{D_1} \right)^2 \right) \quad (6)$$

$$:= A_1 \Delta p A_{eff}(x),$$

where v_1 is the inlet flow velocity.

For real geometries, one might find the effective area curve by either CFD computations or measurements. Once such a curve is obtained, the lift vs. pressure curve is computed by solving the static force equilibrium

$$s(x + x_0) = A_{eff}(x) A_1 \Delta p, \quad (7)$$

The slope of the curve can be obtained by implicit differentiation:

$$\frac{dx}{d\Delta p} = \frac{1}{\Delta p} \frac{A_{eff}(x)}{A'_{eff}(x) - \frac{s}{\Delta p A_1}}, \quad (8)$$

more importantly, at the opening point ($x = 0$) we have $A_{eff}(0) = 1$, hence

$$\left. \frac{dx}{d\Delta p} \right|_{x=0} = \frac{1}{\Delta p} \frac{1}{A'_{eff}(0) - \frac{s}{p_{set} A_1}} = \frac{1}{\Delta p} \frac{1}{A'_{eff}(0) - \frac{1}{x_0}}. \quad (9)$$

Let us consider the following example: $D_1 = 2'' = 51$ mm, $s = 120$ kN/m, $p_{set} = 3$ bar, thus the spring precompression is $x_0 = 5.1$ mm. To highlight the effect of the effective area curve, we consider two synthetic shapes: $A_{eff,1} = 1 + 1.91 \tilde{x}^2$ (valve 1, the black curve in inset (a) of Fig. 2 and $A_{eff,2} = 1 + 1.91 \sqrt{\tilde{x}}$, valve 2, the blue curve in Fig. 2(a)).

Fig. 2 depicts the behaviour of these two valves – see the upper-left panel (a) – via simulating a hypothetical relief event. Consider the lower-right panel (d), where the

red dashed line is the inlet pressure of the valve: in 0.2 seconds, it linearly increases to 60% beyond the set pressure, then it also linearly decreases in another 0.2 seconds to the set pressure and keeps the trend beyond that up to 0.5 seconds. Panel (b) depicts the static curves obtained through solving Eq. (7) (dashed lines) overlaid with the results of the dynamic simulation. Notice how the black curve follows the static characteristic while opening, then, at the turning point, it jumps to a fully open position. When closing, the valve closes at approx. 20% overpressure and undergoes several impacts before closing fully. The other (blue) valve jumps open immediately and stays open up to approx. –20% overpressure (that is, blowdown), before closing. The turning points are clearly defined the intersection of spring rate and Eq. (8), as shown in the lower left panel. It is clear that the static curve plays a crucial role even under dynamic performance, however, the question remains, how to design valves that exhibit the characteristics of valve 2 (blue lines) rather than valve 1 (black line).

2.3 The effect of nozzle ring in the absence of the skirt

Industrial valves often include a nozzle ring (see Fig. 1), which is used to fine-tune and adjust the valve's blowdown (or reseal) pressure, being the difference between the pressure at which the valve opens and the pressure at which it reseats following pressure relief. (Steam valves can even have two rings: a nozzle ring for blowdown adjustment and a nozzle ring for fine-tuning the opening time of the valve.)

Based on the previous section, there is a clear connection between the effective area (that is, the force vs. lift curve) and the blowdown value. In this section, we provide a qualitative explanation for the effect of the blowdown ring and, hence, the effective area curve.

Consider the simplified valve layout in Fig. 1, which depicts a disc valve with D_1 , D_1' , and D_2 nozzle inner, trimmed inner and outer diameter and D_3 , D_4 nozzle ring diameters. The nozzle ring setting will be denoted by x_n , with $x_n = 0$ being the case when it is set to its uppermost position. In what follows, we provide an analytical derivation for the pressure distribution beneath the disc, which will allow us to estimate the pressure force.

Let r denote the radial coordinate, then the flow velocity in the concentric gap is

$$v(r) = \frac{\dot{m}}{\rho A(r)} = \frac{\dot{m}}{\rho r \pi x}. \quad (10)$$

We assume that the total pressure $p(r) + \frac{\rho}{2} v^2$ is constant. Remarkably, the dynamic pressure distribution is independent of the valve opening:

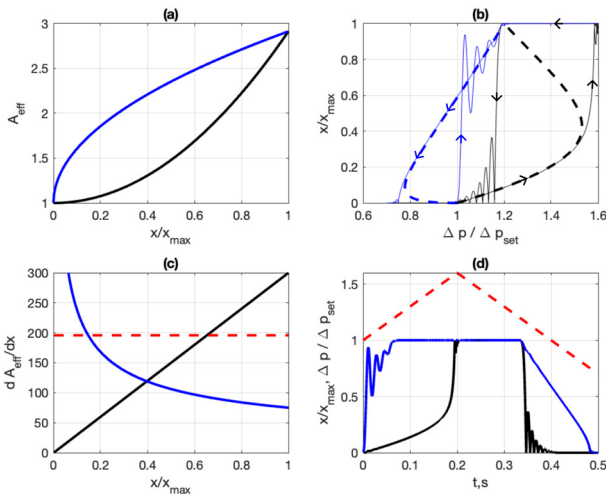


Fig. 2 (a) Effective area curves: $A_{eff,1} = 1 + 1.91 \tilde{x}^2$ (black, valve 1) and $A_{eff,2} = 1 + 1.91 \sqrt{\tilde{x}}$ (blue, valve 2). (b) Equilibrium pressure-lift curves (solid dashed) with the result of dynamic simulations (solid thin lines) in (d), with arrows indicating the opening and closing cycles of the valve. (c) The slope of the curve described by Eq. (8) and the spring precompression (dashed red line). The intersection defines the inflection curves (vertical slope) in (b). (d) Driving pressure (red dashed) and valve lift time histories.

$$\frac{\rho}{2} v(r)^2 = C_d(x)^2 \frac{D_2^2}{r^2} \Delta p. \quad (11)$$

At $r = \frac{D_{out}}{2}$ diameter, the diverging channel ends, hence $p(r) + \frac{\rho}{2} v(r)^2 = \frac{\rho}{2} v_{out}^2$ (the static pressure p_{out} being zero), giving

$$p(r) = C_d(x)^2 \Delta p \left[\left(\frac{D_2}{D_{out}} \right)^2 - \left(\frac{D_2}{2r} \right)^2 \right]. \quad (12)$$

The net (negative) force due to the pressure distribution is obtained by integrating the above pressure distribution between $r = D_1$ and $r = D_{out}$:

$$\begin{aligned} F &= \int_{D_1}^{D_{out}} p(r) 2r\pi dr \\ &= \frac{D_2^2 \pi}{4} \Delta p 2C_d(x)^2 \left[2(1 - \delta^2) + \ln \delta \right] \end{aligned} \quad (13)$$

with $\delta = D_1/D_{out}$. Assuming that the approximate pressure distribution is

$$p(r) = \begin{cases} \Delta p & \text{if } r < D_1 \\ p(r) & \text{if } D_1 < r < D_{out} \end{cases} \quad (14)$$

the corrected effective area curve is

$$\begin{aligned} A_{eff}(x) &= \left(\frac{D_2}{D_1} \right)^2 \left(1 - 2C_d(x)^2 \left[2(1 - \delta^2) + \ln \delta \right] \right) \\ &+ 2C_d(x)^2 \left(\frac{4x}{D_1} \right)^2. \end{aligned} \quad (15)$$

The above formula provides a general description for the effective area curve in the presence of a nozzle ring, which controls the (jet) outlet diameter from D_2 (lowest nozzle ring setting) to D_4 (uppermost nozzle ring position). For a thin-walled piping ($D_1 \approx D_2$) without nozzle ring ($D_{out} = D_1$), we regain the effective area curve defined by Eq. (6). In the general case, the additional correction term (including δ) will add a constant vertical shift to the effective area curve, resulting in negative values for small openings.

2.4 The effect of the skirt

The presence of the skirt (see Fig. 1) changes the flow pattern fundamentally as it breaks the fluid jet, as depicted in Fig. 3. In this case, a two-orifice model gives a more realistic estimation of the pressure distribution and, hence, the fluid force. The two orifices are (a) from cross sections 1 to 2 with loss coefficient ζ_{12} with flow rate Q_{12} and (b) under the skirt with loss coefficient ζ_{34} and flow rate Q_{34} . The corresponding outlet cross sections are $A_2 = D_2\pi x$ and $A_4 = D_2\pi(x + x_b)$. Let p_3 denote the intermediate pressure in

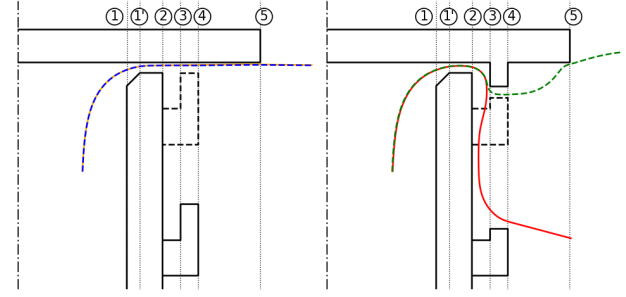


Fig. 3 Streamlines without (left panel) and with (right panel) the skirt, for two adjustment ring settings

the inner chamber (between points 2 and 3). By assuming Borda-Carnot loss at both locations, we have

$$Q_{12} = D_2\pi x \sqrt{\frac{2}{\rho} (\Delta p - p_{sk})} \quad \text{and} \quad (16)$$

$$Q_{34} = D_4\pi (x + x_b) \sqrt{\frac{2}{\rho} p_{sk}}$$

from which we have

$$p_{sk} = \frac{\Delta p}{1 + \left(\frac{D_4}{D_2} \right)^2 \frac{x + x_b}{x}}. \quad (17)$$

Note that for $x = 0$, we have $p_{sk} = \Delta p$ and for increasing x values, we have $\lim_{x \rightarrow \infty} \frac{x + x_b}{x} = 1$. However, the "chamber approximation" breaks down if $x \gg x_s$ (where x_s is the height of the skirt). Assuming that the approximate pressure distribution is

$$p(r) = \begin{cases} \Delta p & \text{if } r < D_2 \\ p_{sk} & \text{if } D_2 < r < D_{out} = D_4 \end{cases}, \quad (18)$$

the pressure force is simply

$$F_p = \frac{D_2^2 \pi}{4} \Delta p + \frac{D_2^2 \pi}{4} \left(\frac{D_4^2}{D_2^2} \left(1 + \frac{x_b}{x} \right) - 1 \right) p_{sk}, \quad (19)$$

hence, after substituting Eq. (17) into Eq. (18), the effective area is ($\delta_{42} = D_4/D_2$)

$$A_{eff,skirt}(x) = 1 + \frac{\delta_{42}^2 - 1}{\delta_{42}^2 \left(1 + \frac{x_b}{x} \right)^2 + 1} + 2C_d(x)^2 \left(\frac{4x}{D_1} \right)^2. \quad (20)$$

3 CFD studies

3.1 Setup

Numerical simulations were carried out in OpenFOAM by applying the steady-state solver SimpleFoam to get the effective area curve of a flat disc valve, as shown in Fig. 4. The numerical domain consisted of a pipe with an inner

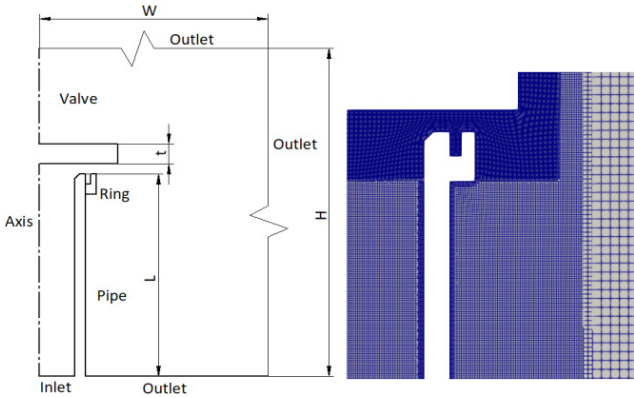


Fig. 4 (Left) Boundary conditions. (Right) Meshing.

diameter of 33.4 mm, an outer diameter of 44.3 mm, and an inlet section of 100 mm. The valve had an outer diameter of 74 mm while its thickness was 25 mm. The total width and height of the domain were 296 mm and 400 mm, respectively. The adjustable ring had an equal thickness as the pipe, with a groove extending from the pipe's edge to the ring's half thickness, while the height of the skirt was 3.73 mm.

The flow is considered axisymmetric; thus, a domain was revolved, and wedge-type boundary conditions were applied for the front and back planes.

Single-phase simulations were run with water (constant density). The meshing set-ups were the same in each simulation, with refinement around the valve body and six boundary layers along the walls of the pipe and the valve. Fixed mean static pressure and zero gradient velocity boundary conditions have been applied for the inlet; total pressure and pressure inlet outlet velocity have been applied for the outlet boundary conditions. k-w-SST turbulence model was chosen with 5% turbulence intensity at the inlet. A steady-state solution was reached when the mean of the vertical component of the force acting on the valve was at 0.1% in the last 100 iterations.

3.2 Discharge coefficient and effective area curves

Fig. 5 depicts the discharge coefficients as a function of the relative gap $4x/D_2$, evaluated according to Eq. (4). For the simple disc geometry (no skirt), the adjustment ring setting has limited influence. As intuitively expected, adding the skirt restricts the flow, and hence, the discharge coefficient is significantly lower in the mid-lift range. For the uppermost ring setting, the C_d values are significantly lower for small openings as well. These findings are consistent (at least for the no-skirt case without ring) with the literature, [7, 12] obtained $C_d = 0.85$ at $\tilde{x} = 0.2$ and $C_d = 0.77$ at $\tilde{x} = 0.4$.

Fig. 6 depicts the effective area curves obtained via CFD, and the corresponding curve fits. Starting with the

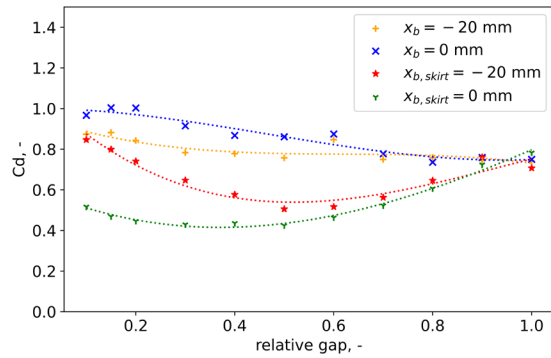


Fig. 5 Discharge coefficients: $x_b = 0$ mm is uppermost adjustment ring position, while $x_b = -20$ mm is the lowermost position (see Fig. 1).

The curve fit parameters are listed in Table 3.

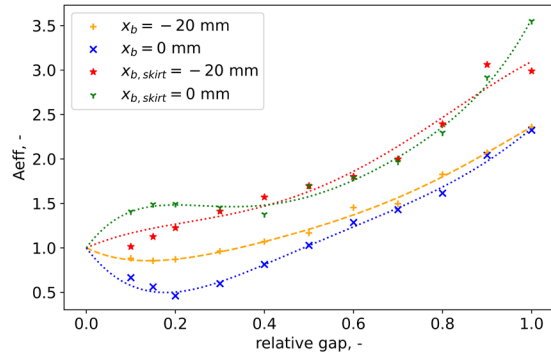


Fig. 6 Effective area curves, the curve fit parameters are listed in Table 2

no-skirt cases, the effective area curves are smaller than 1 for small openings – as predicted by Eq. (15). These cases are similar to the behaviour of a poppet valve, for which the momentum force is also negative for small openings, resulting in decreasing fluid force close to the opening.

The presence of the skirt results in the opposite behaviour: for small openings, the effective area increases, as predicted by Eq. (20). Moreover, it is also clear that in the upper position of the adjustment ring $x_b = 0$ (mm, see Fig. 1), the effect is more profound, which is also supported by engineering experience, see [8, 14].

3.3 Detailed analysis of the flow field

In this section, we provide a detailed analysis of the flowfield for the four cases (skirt/no-skirt, upper/lower ring setting) and explain the effective area curves depicted in Figs. 6–8 depict the total pressure (upper panel), static pressure (middle panel) and velocity (lower panel) distributions for these ring and skirt settings. For convenience, all the depicted quantities are rescaled to fall between 0 and 1.

One of the key findings is that even if the ring is in its top position, the total pressure remains constant up to the

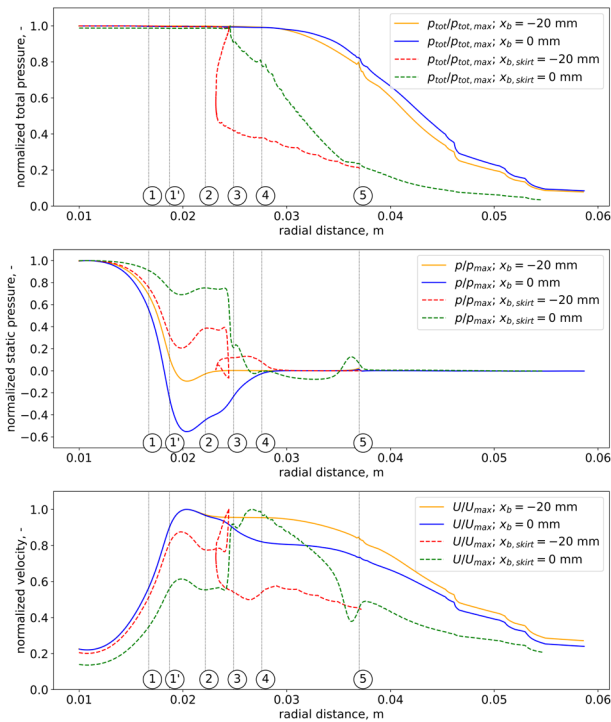


Fig. 7 Comparison of total pressure, static pressure and velocity distributions for small opening $\tilde{x} = 0.2$ for two x_b adjustment ring settings (see Fig. 1)

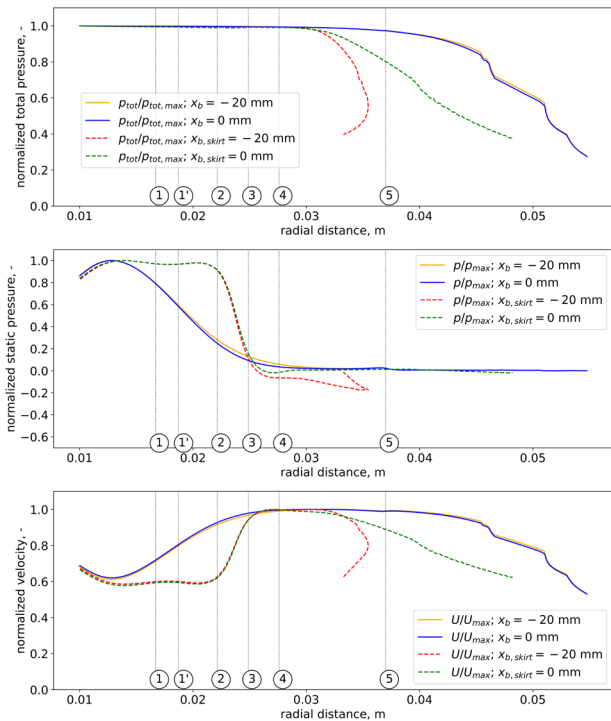


Fig. 8 Comparison of total pressure, static pressure and velocity distributions close to full lift, $\tilde{x} = 0.9$, for two x_b adjustment ring settings (see Fig. 1).

exit diameter D_4 for all cases. This means that the flow is practically ideal up to the exit point, which justifies the

assumptions of Section 2 and allows using Bernoulli's theorem to estimate the pressure distribution.

Let us start with the no-skirt case (yellow and blue curves). The static pressure – as estimated by Eq. (14) – is lower than the ambient pressure in the outer regions (between diameters 2–4). This is simply because the flow is decelerating through the gap (the flow cross-section increases as the radius increases), and thus, the pressure also increases radially and finally reaches the ambient pressure at D_{out} (middle and lower panels, yellow and blue curves between points 2 and 4). In the inner part of the domain, the static pressure drops from the inner Δp value to negative values due to the acceleration of the fluid (middle and lower panels, blue and yellow curves between points 1 and 2). It is also clear from the middle panel that the lower the adjustment ring is set, the smaller the negative pressure is and hence, the effective area increases, as it was shown in Fig. 6. For large openings, both the negative-pressure regions and the effect of the adjustment ring vanishes consistently with Eq. (14) and Fig. 6.

The presence of the skirt changes the pressure field drastically. Due to the large deflection of the flow, the pressure distribution does not fall beyond the outer pressure (see the red and green dashed lines in the middle pane), and under the whole disc, the pressure is positive, resulting in a higher overall pressure force. Note that this case is correctly captured by the "two-orifice" model described in Section 2.4. The theory also correctly captures the effect of the nozzle ring: the upper ring setting (green dashed line in the middle pane) results in higher static pressure and, hence, higher effective area value than the lower ring setting (red dashed line). Note that the higher overall fluid force (especially at small openings) is *not* due to the deflection angle as suggested by many studies but due to the higher static pressure values at outer diameters.

Fig. 8 depicts the same graphs in the case of large valve opening ($\tilde{x} = 0.9D_1/4$). It is clear that at such lifts, the influence of the nozzle ring position is negligible. Also, having a look at the middle pane (static pressure distribution) reveals that the overall pressure force is higher in the case of the disc with a skirt, resulting again in higher overall force, which was clearly seen in Fig. 6.

4 Valve dynamics with realistic effective area curves

Finally, we rerun the previous computations presented in Fig. 2 with synthetic effective curves, now with the ones obtained with the CFD computation. The actual simulation data are provided in Table 1. The damping coefficient was chosen to be 1% of the critical damping ($k_{crit} = 2m\omega$, $\omega = \sqrt{s/m}$ being the natural frequency of

Table 1 Data used for simulations

D_1	s	x_{max}	m	k
51 mm	120 kN/m	$D_1/4$	0.442 kg	46 Ns/m

the valve). The curve fit for the effective area and discharge coefficient values are in the form of

$$A_{eff}(\tilde{x}) = \sum a_i \tilde{x}^i \quad \text{and} \quad C_d(\tilde{x}) = \sum b_i \tilde{x}^i, \quad (21)$$

with $x = 4x/d = x/x_{max}$ and parameters a_i and b_i are listed in Tables 2 and 3. It should be noted, however, that the discharge coefficient values are not needed to generate the simulation results as we are not presenting actual flow rates.

Fig. 9 depicts the simulation results with $p_{set} = 3$ bar. If the adjustment ring is in its lower-most position (black curves), the opening is almost proportional and fairly slow. Once the valve reaches the inflexion point (approx. at $x/x_{max} = 0.45$), it "jumps" open. Upon closing, this valve closes at approx. 5% of the set pressure, which is clearly undesired behaviour. With the upper-most adjustment ring setting, the valve behaviour is significantly different. First of all, as $dA_{eff}/dx > 1/x_0$, the initial slope is positive – see panel (b) and Eq. (9) – the valve exhibits a popping action up to 20% of the full lift, after which it opens proportionally before jumping again at 50% lift. More importantly, the valve closes at approx. 95% of the set pressure, resulting in the expected blowdown behaviour.

Fig. 10 presents the same simulation results with $p_{set} = 5$ bar, which was achieved by adjusting the spring precompression. It is important to notice that – as described by Eq. (7) – such change in the precompression also changes the equilibrium curves (panel (b)) and hence the opening and blowdown characteristics. It is particularly striking how drastically the blowdown changes.

Table 2 Curve fit parameters for A_{eff} curves

geometry	a_5	a_4	a_3	a_2	a_1	a_0
x_{b-20}	-7.003	20.49	22.24	12.53	-2.407	1
x_{b0}	-8.28	32.1	-44.58	28.82	-6.71	1
$x_{b-20,skirt}$	0	-5.77	12.14	-6.46	2.18	1
$x_{b0,skirt}$	25.71	-70.47	74.87	-34.35	6.82	1

Table 3 Curve fit parameters for curves

geometry	b_3	b_2	b_1	b_0
x_{b-20}	-0.73	1.36	-0.86	0.96
x_{b0}	0.59	-0.83	-0.014	1
$x_{b-20,skirt}$	-1.13	3.21	-2.41	1.09
$x_{b0,skirt}$	-0.38	1.63	-1.05	0.6

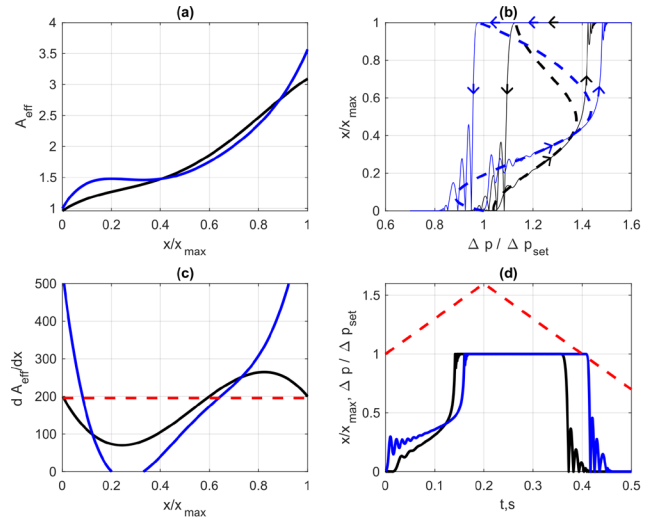


Fig. 9 Simulation results with $p_{set} = 3$ bar. (a) Effective area curves obtained from CFD computations (with a skirt, see Fig. 6). The blue line refers to the uppermost position of the adjustment ring, while the black line refers to the lowermost position. (b) Equilibrium pressure-lift curves (solid dashed) with the result of dynamic simulations in (d), with arrows indicating the opening and closing cycles of the valve. (c) The slope of the curve described by Eq. (8) and the spring precompressions (dashed red line). The intersection defines the inflexion curves (vertical slope) in (b). (d) Driving pressure (red dashed) and valve lift time histories.

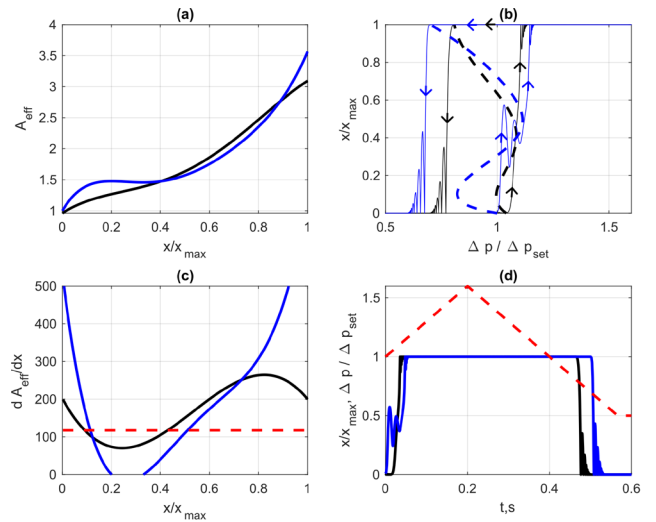


Fig. 10 Simulation results with $p_{set} = 5$ bar, similar to Fig. 9.

5 Conclusion

This study provided a detailed analysis of relief valve behaviour. Notably, we presented a qualitative and quantitative analysis of the blowdown phenomena. The key findings are as follows.

- The effective area curve plays a central role in the pressure vs. lift characteristic curve of the valve and allows the estimation of both opening (popping) behaviour and closing (blowdown) characteristics.

- The nozzle ring in itself is insufficient for exhibiting blowdown; the skirt (strong backward deflection of the flow) plays an indispensable role.
- The blowdown behaviour (especially at small openings) is not caused by the deflected flow angle (momentum force) but is due to the "second orifice" effect that results in higher static pressure distribution behind the valve body.

Our CFD computations showed that the effective area curve is sensitive to geometry thus it might be challenging to provide an accurate prediction via CFD. Moreover, the static pressure-lift characteristics of the same valve (with the same effective area curve) vary with varying set pressure and/or spring stiffness, which explains the widely known practice that one particular valve needs different ring settings when the same (relative) blowdown must be set at different set pressures. We also emphasize that, because of the Coanda effect, bi-stable regions and fluid force fluctuations might arise, which makes the measurements or CFD computations challenging.

References

- [1] Herink, T., Doskočil, J., Růžička, M., Henry, P. A., Sadowski, R. A., Zámotný, P. "Propylene column pressure relief valves chattering resulting in explosion and fire of the Steam Cracker unit", *Journal of Loss Prevention in the Process Industries*, 74, 104658, 2022. <https://doi.org/10.1016/j.jlp.2021.104658>
- [2] Singh, A. "An analytical study of the dynamics and stability of a spring loaded safety valve", *Nuclear Engineering and Design*, 72(2), pp. 197–204, 1982. [https://doi.org/10.1016/0029-5493\(82\)90215-1](https://doi.org/10.1016/0029-5493(82)90215-1)
- [3] Ray, A. "Dynamic modeling and simulation of a relief valve", *Simulation*, 31(5), pp. 167–172, 1978. <https://doi.org/10.1177/003754977803100504>
- [4] Darby, R. "The dynamic response of pressure relief valves in vapor or gas service, part I: Mathematical model", *Journal of Loss Prevention in the Process Industries*, 26(6), pp. 1262–1268, 2013. <https://doi.org/10.1016/J.JLP.2013.07.004>
- [5] Aldeeb, A. A., Darby, R., Arndt, S. "The dynamic response of pressure relief valves in vapor or gas service. Part II: Experimental investigation", *Journal of Loss Prevention in the Process Industries*, 31, pp. 127–132, 2014. <https://doi.org/10.1016/J.JLP.2014.06.002>
- [6] Darby, R., Aldeeb, A. A. "The dynamic response of pressure relief valves in vapor or gas service. Part III: Model validation", *Journal of Loss Prevention in the Process Industries*, 31, pp. 133–141, 2014. <https://doi.org/10.1016/J.JLP.2014.06.001>
- [7] Johnston, D. N., Edge, K. A., Vaughan, N. D. "Experimental Investigation of Flow and Force Characteristics of Hydraulic Poppet and Disc Valves", *Proceedings of the Institution of Mechanical Engineers, Part A: Journal of Power and Energy*, 205(3), pp. 161–171, 1991. https://doi.org/10.1243/PIME_PROC_1991_205_025_02
- [8] Song, X. G., Park, Y. C., Park, J. H. "Blowdown prediction of a conventional pressure relief valve with a simplified dynamic model", *Mathematical and Computer Modelling*, 57(1–2), pp. 279–288, 2013. <https://doi.org/10.1016/j.mcm.2011.06.054>
- [9] Song, X., Cui, L., Cao, M., Cao, W., Park, Y., Dempster, W. M. "A CFD analysis of the dynamics of a direct-operated safety relief valve mounted on a pressure vessel", *Energy Conversion Management*, 81, pp. 407–419, 2014. <https://doi.org/10.1016/j.enconman.2014.02.021>
- [10] Song, X. G., Wang, L. T., Park, Y. C., Sun, W. "A Fluid-structure Interaction Analysis of the Spring-Loaded Pressure Safety Valve during Popping Off", *Procedia Engineering*, 130, pp. 87–94, 2015. <https://doi.org/10.1016/J.PROENG.2015.12.178>
- [11] Yang, L., Wang, Z., Dempster, W., Yu, X., Tu, S. T. "Experiments and transient simulation on spring-loaded pressure relief valve under high temperature and high pressure steam conditions", *Journal of Loss Prevention in the Process Industries*, 45, pp. 133–146, 2017. <https://doi.org/10.1016/j.jlp.2016.11.019>
- [12] Duan, Y., Jackson, C., Eaton, M. D., Bluck, M. J. "An assessment of eddy viscosity models on predicting performance parameters of valves", *Nuclear Engineering and Design*, 342, pp. 60–77, 2019. <https://doi.org/10.1016/J.NUCENGDDES.2018.11.036>
- [13] Zong, C., Zheng, F., Chen, D., Dempster, W., Song, X. "Computational Fluid Dynamics Analysis of the Flow Force Exerted on the Disk of a Direct-Operated Pressure Safety Valve in Energy System", *Journal of Pressure Vessel Technology*, 142(1), PVT-19-1128, 2020. <https://doi.org/10.1115/1.4045131>
- [14] Zhang, J., Yang, L., Dempster, W., Yu, X., Jia, J., Tu, S. T. "Prediction of blowdown of a pressure relief valve using response surface methodology and CFD techniques", *Applied Thermal Engineering*, 133, pp. 713–726, 2018. <https://doi.org/10.1016/j.applthermaleng.2018.01.079>

Finally, it must be noted that the real challenge is the reverse engineering of the effective area curve into a real geometry; i.e. one can relatively easily translate a prescribed pressure-lift curve (obtained by higher-level engineering decision) into an effective area curve; however, finding the actual valve geometry that exhibits that curve seems to be cumbersome; developing such a tool would revolutionize valve design.

Acknowledgement

Project no. KDP-IKT-2023-900-II-00000957/0000003 has been implemented with the support provided by the Ministry of Culture and Innovation of Hungary from the National Research, Development and Innovation Fund, financed under the KDP-2023 funding scheme.

The scientific work/research and/or results publicised in this article was reached with the sponsorship of Gedeon Richter Talentum Foundation in framework of Gedeon Richter Excellence PhD Scholarship of Gedeon Richter.

- [15] Ye, Z.-H., Li, W.-Q., Xu, Y.-X., Jin, Z.-J., Qian, J.-Y. "Effects of adjusting ring and spring stiffness on fluid dynamics of steam spring-loaded safety valve", *Nuclear Engineering and Technology*, in press. (Accepted for publication November 2024)
<https://doi.org/10.1016/J.NET.2024.11.040>
- [16] Allison, T. C., Brun, K. "Testing and Modeling of an Acoustic Instability in Pilot-Operated Pressure Relief Valves", *Journal of Engineering for Gas Turbines and Power*, 138(5), GTP-15-1279, 2016.
<https://doi.org/10.1115/1.4031623>
- [17] Burhani, M. G., Hős, C. "An Experimental and Numerical Analysis on the Dynamical Behavior of a Safety Valve in the Case of Two-phase Non-flashing Flow", *Periodica Polytechnica Chemical Engineering*, 65(2), pp. 251–260, 2021.
<https://doi.org/10.3311/PPCh.16262>
- [18] Dempster, W., Alshaikh, M. "An Investigation of the Two Phase Flow and Force Characteristics of a Safety Valve", *Procedia Engineering*, 130, pp. 77–86, 2015.
<https://doi.org/10.1016/J.PROENG.2015.12.177>
- [19] Singh, A. "On the stability of a coupled safety valve-piping system", In: 2. International Topical Meeting on Nuclear Reactor Thermal Hydraulics (ANS), Santa Barbara, CA, USA, 1983, pp. 929–937. ISBN: 0-89448-110-X
- [20] Urata, E. "Thrust of Poppet Valve", *Bulletin of JSME*, 12(53), pp. 1099–1109, 1969.
<https://doi.org/10.1299/JSME1958.12.1099>
- [21] Maeda, T. "Studies on the Dynamic Characteristic of a Poppet Valve: 1st Report, Theoretical Analysis", *Bulletin of JSME*, 13(56), pp. 281–289, 1969.
<https://doi.org/10.1299/JSME1958.13.281>
- [22] Páez Chávez, J., Wiercigroch, M. "Bifurcation analysis of periodic orbits of a non-smooth Jeffcott rotor model", *Communications in Nonlinear Science and Numerical Simulation*, 18(9), pp. 2571–2580, 2013.
<https://doi.org/10.1016/J.CNSNS.2012.12.007>
- [23] Bazsó, C., Hos, C. "On the Static Instability of Liquid Poppet Valves", *Periodica Polytechnica Mechanical Engineering*, 59(1), pp. 1–7, 2015.
<https://doi.org/10.3311/PPME.7049>
- [24] Wu, D., Burton, R., Schoenau, G. "An Empirical Discharge Coefficient Model for Orifice Flow", *International Journal of Fluid Power*, 3(3), pp. 13–19, 2002.
<https://doi.org/10.1080/14399776.2002.10781143>
- [25] Kawashima, K., Kagawa, T., Fujita, T. "Instantaneous Flow Rate Measurement of Ideal Gases", *Journal of Dynamic Systems, Measurement, and Control*, 122(1), pp. 174–178, 2000.
<https://doi.org/10.1115/1.482439>
- [26] MacLeod, G. "Safety Valve Dynamic Instability: An Analysis of Chatter", *Journal of Pressure Vessel Technology*, 107(2), pp. 172–177, 1985.
<https://doi.org/10.1115/1.3264430>
- [27] Botros, K. K., Dunn, G. H., Hrycyk, J. A. "Riser-Relief Valve Dynamic Interactions", *Journal of Fluids Engineering*, 119(3), pp. 671–679, 1997.
<https://doi.org/10.1115/1.2819297>
- [28] Izuchi, H. "Stability Analysis of Safety Valve", In: 2010 AIChE Spring Meeting and Global Congress on Process Safety, San Antonio, TX, USA, 2010. [online] Available at: https://www.researchgate.net/publication/267358621_Stability_Analysis_of_Safety_Valve (Accessed: 11 Jan 2025)